

# The structural evolution in transitional nuclei of mass $80 \leq A \leq 132$

M. Bhuyan\*

State Key Laboratory of Theoretical Physics, Institute of Theoretical Physics, Chinese Academy of Sciences, Beijing 100190, China  
(Dated: December 3, 2024)

In this theoretical study, we report an investigation on the behavior of two neutron separation energy, differential variation of the separation energy and the abnormality in nuclear charge radius along the isotopic and isotonic chains of transition nuclei. We have used relativistic mean field formalism with NL3 and NL3\* forces for this present analysis. The study refers to *even-even* nuclei such as Zr, Mo, Ru and Pd with  $N = 40 - 86$ , where a rich collective phenomena such as proton radioactivity, cluster or nucleus radioactivity, exotic shapes, *Island of Inversion* and etc. are observed. These non-monotonic aspects over the isotopic chain are mainly correlated with the structural properties like shell/sub-shell closures, shape transition, clustering and magicity etc. In addition to these, we have shown the internal configuration of these nuclei to get a further insight into the reason for these discrepancies.

PACS numbers: 21.10.Dr, 21.10.Ft, 21.10.Gv, 21.10.Tg

## I. INTRODUCTION

Nowadays, one of the most sensitive and crucial region in the nuclear chart for investigation is laying in between  $Z=35-64$  and  $A=82-132$ . This region reveals a large number of interesting discoveries of new phenomena, such as proton radioactivity [1–3], cluster or nucleus radioactivity [4–6], exotic shapes [7, 8], *Island of inversion* [9, 10], abnormal variation of major shell closures (i.e. extra stability near drip-line) [11–13] and giant halo near neutron drip-line region [14] etc. These crucial features may be due to the rapid growing possibility of neutron-proton ratio ( $N/Z$ ) in a nucleus. From last few decades, it is possible to study these exotic nuclei by using the radioactive isotope beams (RIB) facilities. This reveals the new concept entitled as *aforementioned* magic number. In other word, the confirmation of magic number near  $\beta$ -stability line are not mandatorily universal [15–17]. Further, the structural properties of nuclei far away from the  $\beta$ -stability line are also an active areas of research in both theories and experiments [13, 14, 18]. In particular, the neutron-rich Zr-, Mo-, Ru- and Pd- with mass numbers  $A=100-130$  are of special interest for various reasons. For example, they lie far away from  $\beta$ -stable region of *Nuclear Landscape*, result in a well established deformation, but close enough in magnitude of microscopic excitations to compete with collectivity of double shell closure nuclei [14, 19, 20]. Moreover, these nuclei are also holding an active participation in the nucleosynthesis of heavy nuclei in astrophysical  $r$ -process. The mass and decay properties are quite essential ingredient to build up the path, the isotopic abundances and the time period of these process [21].

In addition to that the nuclear structure of these nuclei are characterized by a strong competition between various shapes, which gives rise to the shape instabilities that lead to coexistence nuclear shape transitions in the isotopic chains [22]. This could be understood from the the potential energy surface at different deformations. Elaborately, the occurrence of

two (or more) nearly equally deep minima in the potential energy surface at different deformations shows the signature for nuclear shape coexistence. Hence, one can say the nuclear shape are not only vary with the nucleon number but also with the excitation energy and spin. It is well known that the binding energy of a nucleus is one of the most precise measured observable from the experiments [23, 24]. Several nuclear observables which are highly relevant for understanding various features of nuclear structure can be computed from its mass such as the average nuclear field, nucleon-nucleon (NN) potential, single particle energy etc. The correlations among these fundamental quantities are emended to explain the deformed ground states, low lying isomeric states and few derived quantities like moments of inertia and vibrational excitation energy etc [25–28]. It is acclaimed that the energy involved in removal of fermions from a strongly correlated system of identical fermions must be a good indicator for the stability of the system. This magnitude of this energy have much higher values for systems with *even* number of particles than *odd* one, if the pairing is a dominant component in the binary *fermion-fermion* interaction.

In this present work, the quantities of interest are the nuclear potential energy surface, nuclear shape, nuclear binding energy, two neutron separation energies ( $S_{2n}$ ), the differential variation of neutron separation energy  $\Delta S_{2n}$  and the root-mean-square charge distribution  $r_{ch}$  for the *even-even* mass transition nuclei. Base on these decisive observables, we have focused on the evolution on the structural properties of transition nuclei. The paper is organized as follows: Section II gives a brief description of the relativistic mean field formalism. The results of our calculation along with discussions are presented in Section III. Section IV includes a short summary along with few concluding remarks.

## II. THE RELATIVISTIC MEAN-FIELD (RMF) METHOD

The microscopic self consistent mean-field calculations are the standard tool for the investigation of nuclear structure phenomena. The relativistic mean field (RMF) theory is one of the most popular and widely used formalism among them.

\*Email: bunuphy@itp.ac.cn

It starts with the basic Lagrangian that describes nucleons as Dirac spinors interacting through different meson fields. The original Lagrangian of Walecka has taken several modifications to take care of various limitations and the successful relativistic Lagrangian density for a nucleon-meson many body system [29–39] is expressed as:

$$\begin{aligned} \mathcal{L} = & \bar{\psi}_i \{ i \gamma^\mu \partial_\mu - M \} \psi_i + \frac{1}{2} \partial^\mu \sigma \partial_\mu \sigma - \frac{1}{2} m_\sigma^2 \sigma^2 \\ & - \frac{1}{3} g_2 \sigma^3 - \frac{1}{4} g_3 \sigma^4 - g_s \bar{\psi}_i \psi_i \sigma - \frac{1}{4} \Omega^{\mu\nu} \Omega_{\mu\nu} \\ & + \frac{1}{2} m_w^2 V^\mu V_\mu - g_w \bar{\psi}_i \gamma^\mu \psi_i V_\mu - \frac{1}{4} \vec{B}^{\mu\nu} \cdot \vec{B}_{\mu\nu} \\ & + \frac{1}{2} m_\rho^2 \vec{R}^\mu \cdot \vec{R}_\mu - g_\rho \bar{\psi}_i \gamma^\mu \vec{\tau} \psi_i \cdot \vec{R}_\mu \\ & - \frac{1}{4} F^{\mu\nu} F_{\mu\nu} - e \bar{\psi}_i \gamma^\mu \frac{(1 - \tau_{3i})}{2} \psi_i A_\mu. \end{aligned} \quad (1)$$

From the above Lagrangian we obtain the field equations for the nucleons and mesons. These equations are solved by expanding the upper and lower components of the Dirac spinors and the boson fields in an axially deformed harmonic oscillator basis, with an initial deformation  $\beta_0$ . The set of coupled equations are solved numerically by a self-consistent iteration method [40–43]. The centre-of-mass motion energy correction is estimated by the usual harmonic oscillator formula  $E_{c.m.} = \frac{3}{4} (41 A^{-1/3})$ . The total quadrupole deformation parameter  $\beta_2$  is evaluated from the resulting proton and neutron quadrupole moments, as

$$Q = Q_n + Q_p = \sqrt{\frac{16\pi}{5}} \left( \frac{3}{4\pi} A R^2 \beta_2 \right). \quad (2)$$

The root mean square (rms) matter radius is defined as

$$\langle r_m^2 \rangle = \frac{1}{A} \int \rho(r_\perp, z) r^2 d\tau, \quad (3)$$

where  $A$  is the mass number, and  $\rho(r_\perp, z)$  is the axially deformed density. The total binding energy and other observables are also obtained by using the standard relations, given in [29]. In order to take care of the pairing effects in the present study, we have used the constant gap for proton and neutron, as given in [44, 45], which are valid for nuclei both on or away from the stability line (more details in Ref. [32]).

### III. DETAILS OF CALCULATION AND RESULTS DISCUSSION

The mean-field equations are solved self-consistently by taking different inputs of the initial deformation called  $\beta_0$  [29, 32, 46–48]. For a normal ground state solution of the considered mass region, the desire number of major shells for fermions and bosons are  $N_F = N_B = 12$ . To verify the convergence of the solutions, few calculations are done with  $N_F = N_B = 12-16$ . The variation of these solutions are  $\leq 0.002\%$  on binding energy and  $0.001\%$  on nuclear radii over the range of major shell. This implies that the used model space is good

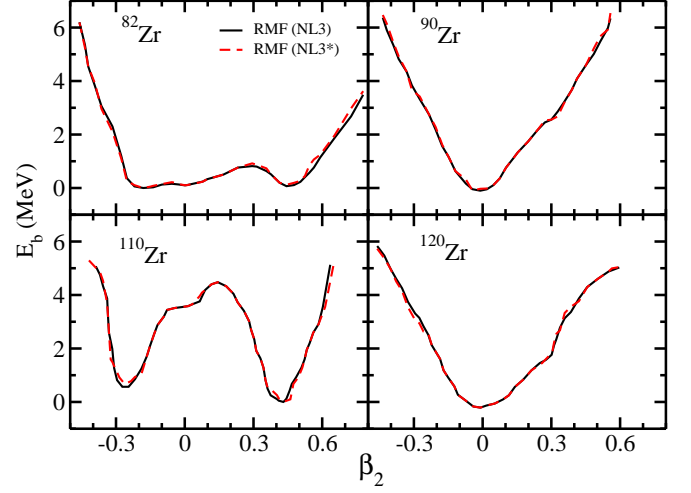


FIG. 1: (Color online) The potential energy surface of  $^{82,90,110,120}\text{Zr}$  as a function of quadrupole deformation parameter  $\beta_2$  for both  $NL3$  and  $NL3^*$  forces in axially deformed relativistic mean field calculations.

enough for the considered mass regions. However, the number of mesh points for Gauss-Hermite and Gauss-Lagurre integration are 20 and 24, respectively. Here, we have used the well known  $NL3$  [46] and recent developed  $NL3^*$  [47] force parameters, which are able to reproduce the properties of the stable nuclei as well as the nuclei away from the  $\beta$ -stability line. We obtain the calculation for different potentials, nuclear densities (for protons and neutrons), single-particle energy for nucleons, nuclear radii, deformation parameter and binding energies etc. For a given nucleus, there are more than one solutions. In this case, the solution corresponding to maximum binding energy is treated as ground state for a given nucleus and other solutions are the intrinsic excited states (see FIG. 1).

#### A. Potential energy surface

Conventionally, in case of a quantum mechanical system, the path followed by the different solutions at various deformation defines a potential barrier or potential energy surface, which can be used for the determination of the ground state of a nucleus. More elaborately, from the potential energy surface (PES) obtained from a self-consistent relativistic mean field theory, one can regulate the reasonable results for the ground state similar to the non-relativistic calculations [49]. Since quadrupole deformation plays the most important and dominant part, we have neglected the other deformation coordinates in the present study for simplicity and low computation time cost. Here, the potential energy curve is calculated microscopically by the constrained RMF theory [32, 33, 50–52]. The expectation value of the Hamiltonian [48, 51, 53] at

TABLE I: The binding energy per particle  $E_B/A$  and the quadrupole deformation parameter  $\beta_2$  for the ground states of transition nuclei compare with the experimental data [54], wherever available.

N	RMF (NL3)			RMF (NL3*)			Experiment			RMF (NL3)			RMF (NL3*)			Experiment		
	BE	$r_{ch}$	$\beta_2$	BE	$r_{ch}$	$\beta_2$	BE	$r_{ch}$	$\beta_2$	BE	$r_{ch}$	$\beta_2$	BE	$r_{ch}$	$\beta_2$	BE	$r_{ch}$	$\beta_2$
<sup>86–114</sup> Zr										<sup>86–114</sup> Ru								
42	691.3	4.29	−0.197	690.9	4.29	−0.192			0.367	698.7	4.39	−0.204	698.1	4.39	−0.199			
	691.0	4.28	0.488	690.6	4.28	0.488												
44	715.7	4.29	−0.188	715.8	4.27	−0.001			0.251	727.0	4.39	0.064	727.0	4.37	0.058			
	715.5	4.28	0.469	715.5	4.28	0.467												
46	739.2	4.28	0.001	739.2	4.27	0.001	740.6		0.151	755.7	4.39	0.096	755.5	4.38	0.089			
48	762.6	4.28	0.001	761.9	4.28	0.001	762.6	4.2812	0.185	782.3	4.37	0.006	782.0	4.37	0.004			
50	783.9	4.28	0.001	783.1	4.28	0.000	783.9	4.2696	0.089	808.0	4.37	0.001	807.4	4.37	0.000	806.9		
52	797.8	4.29	0.001	797.2	4.28	0.000	799.8	4.3057	0.1027	825.6	4.39	0.003	825.1	4.38	0.002	826.5	4.3927	0.1579
54	810.5	4.34	0.169	808.9	4.31	0.002	814.7	4.3312	0.090	843.2	4.42	0.159	842.5	4.42	0.155	844.8	4.4232	0.1947
56	824.5	4.38	0.243	822.9	4.38	0.233	828.9	4.3498	0.080	860.1	4.45	0.205	859.2	4.44	0.199	861.9	4.4536	0.2148
58	837.0	4.42	0.318	834.9	4.40	0.274	840.9	4.4185		875.3	4.47	0.225	874.3	4.47	0.216	877.9	4.4818	0.2404
60	849.8	4.48	0.432	847.6	4.49	0.453	852.4	4.5220	0.355	889.3	4.49	0.234	888.2	4.48	0.215	893.0	4.5104	0.2707
62	860.6	4.50	0.428	858.2	4.50	0.428	863.7	4.5690	0.427	903.9	4.57	0.385	901.7	4.52	0.295	907.5		0.257
64	870.6	4.52	0.427	868.0	4.52	0.424			0.38	917.6	4.54	−0.236	916.3	4.53	−0.232	920.9		0.292
										916.9	4.58	0.373	915.8	4.57	0.371			
66	880.4	4.54	0.419	877.6	4.54	0.418				931.0	4.55	−0.236	929.5	4.55	−0.234	933.3		0.295
										929.1	4.59	0.357	928.0	4.59	0.357			
68	889.8	4.56	0.416	886.8	4.56	0.419				943.4	4.57	−0.239	941.5	4.57	−0.238	945.0		0.306
										941.5	4.60	0.349	940.1	4.60	0.348			
70	897.2	4.59	0.445	893.9	4.59	0.461				954.1	4.59	−0.233	951.8	4.58	−0.229			
72	904.1	4.62	0.478	900.4	4.62	0.479				963.9	4.59	−0.203	961.5	4.59	−0.196			
74	911.8	4.52	−0.170	908.8	4.52	−0.166				974.2	4.61	−0.178	971.5	4.60	−0.176			
76	917.7	4.52	−0.109	914.5	4.52	−0.095				983.1	4.62	−0.169	979.9	4.61	−0.167			
78	923.4	4.52	0.065	920.0	4.52	0.043				991.6	4.61	0.114	988.7	4.60	0.111			
80	929.5	4.54	0.002	925.7	4.53	0.002				999.5	4.61	0.074	996.2	4.61	0.074			
82	935.5	4.55	0.000	931.0	4.55	0.001				1007.3	4.62	0.001	1003.4	4.61	0.001			
84	936.3	4.56	0.003	931.8	4.56	0.009				1010.1	4.64	0.067	1006.3	4.64	0.076			
86	936.9	4.57	0.062	932.5	4.57	0.067				1013.2	4.67	0.139	1009.3	4.66	0.136			

certain deformation is given as,

$$H' = \sum_{ij} \frac{\langle \psi_i | H_0 - \lambda Q_2 | \psi_j \rangle}{\langle \psi_i | \psi_j \rangle}, \quad (4)$$

where  $\lambda$  is the constraint multiplier and  $H_0$  is the Dirac mean field Hamiltonian. The convergence of the numerical solutions on the binding energy and the deformation are not very much sensitive to the deformation parameter  $\beta_0$  of the harmonic oscillator basis for the considered range due to the large basis. Thus the deformation parameter  $\beta_0$  of the harmonic oscillator basis is chosen near the expected deformation to obtain high accuracy and less computation time period.

The potential energy surface as a function of deformation

parameter  $\beta_2$ , for the proton rich nucleus <sup>82</sup>Zr, the double magic nucleus <sup>90</sup>Zr and the neutron rich nucleus <sup>110,120</sup>Zr are shown in Fig. 1, as a representative case. All other *Mo*–, *Ru*– and *Pd*– isotopes are also showing the similar behaviors, which are not given here. The energy ( $E_b = E_{g.s} - E_{e.s}$ ) on the *Y*–axis is the difference between the ground state energy to other constraint energy solutions. The solid and dotted line in the figure are for *NL3* and *NL3\** force, respectively. The calculated *PES* for both the cases are shown for a wide range from oblate to prolate deformations. We notice from the figure that there are more than one minima appear at different  $\beta_2$ . The magnitude of binding energy for the corresponding minima shows that the ground state solution appear at a cer-

TABLE II: Same as Table I, only for  $^{86-114}\text{Mo}$  and  $^{86-114}\text{Pd}$  isotopes.

N	RMF (NL3)			RMF (NL3*)			Experiment			RMF (NL3)			RMF (NL3*)			Experiment		
	BE	$r_{ch}$	$\beta_2$	BE	$r_{ch}$	$\beta_2$	BE	$r_{ch}$	$\beta_2$	BE	$r_{ch}$	$\beta_2$	BE	$r_{ch}$	$\beta_2$	BE	$r_{ch}$	$\beta_2$
$^{86-114}\text{Mo}$										$^{86-114}\text{Pd}$								
42	696.7	4.34	-0.206	696.2	4.34	-0.203				697.8	4.42	0.002	697.8	4.42	0.002			
44	722.2	4.32	0.001	719.5	4.32	0.002	725.8			730.0	4.44	0.094	729.9	4.44	0.095			
46	748.2	4.33	0.003	748.2	4.33	0.003	750.1			760.9	4.43	0.101	760.7	4.43	0.104			
48	773.4	4.33	0.001	773.1	4.33	0.001	773.7			789.5	4.42	0.004	789.1	4.42	0.005			
50	796.9	4.33	0.001	796.4	4.33	0.001	796.5	4.3156	0.1058	817.4	4.42	0.001	816.8	4.41	0.001	815.0		
52	812.7	4.34	0.001	812.2	4.34	0.001	814.2	4.3518	0.1509	836.9	4.43	0.003	836.3	4.42	0.004	836.3		
54	828.1	4.38	0.174	827.1	4.37	0.158	830.8	4.3841	0.1720	855.9	4.46	0.136	855.4	4.46	0.139	856.4		
56	843.5	4.42	0.230	842.2	4.41	0.220	846.2	4.4088	0.1683	874.2	4.48	0.176	873.6	4.48	0.177	875.3	4.4839	0.196
58	857.2	4.45	0.268	855.7	4.43	0.246	860.5	4.4458	0.2309	891.1	4.51	0.189	890.5	4.50	0.188	892.8	4.5086	0.209
60	871.2	4.50	0.366	869.1	4.49	0.356	873.9		0.311	906.9	4.52	0.187	906.2	4.52	0.184	909.5	4.5322	0.229
62	883.6	4.53	0.386	881.4	4.52	0.382	886.9		0.362	921.8	4.53	0.190	921.1	4.53	0.179	925.2	4.5563	0.243
64	895.4	4.49	-0.234	894.0	4.49	-0.228	898.9		0.354	936.1	4.57	0.240	934.9	4.54	0.165	940.2	4.5776	0.257
	895.2	4.54	0.379	893.9	4.54	0.377												
66	907.4	4.51	-0.236	905.7	4.51	-0.233			0.38	951.8	4.59	-0.231	950.4	4.58	-0.229	954.3		0.220
	906.5	4.56	0.374	904.9	4.55	0.373				950.3	4.60	0.292	949.5	4.60	0.290	77		
68	918.1	4.53	-0.241	915.9	4.53	-0.239				965.7	4.62	-0.23	963.9	4.60	-0.234	967.6		0.164
										963.5	4.62	0.304	961.9	4.60	0.301			
70	927.0	4.55	-0.231	924.6	4.54	-0.223				977.9	4.63	-0.221	975.8	4.61	-0.226			0.207
										975.3	4.60	0.216	974.1	4.59	0.216			
72	935.7	4.55	-0.197	933.2	4.55	-0.190				989.1	4.63	-0.198	986.8	4.62	-0.184			
74	944.6	4.57	-0.180	941.7	4.56	-0.179				1000.6	4.63	-0.163	998.1	4.62	-0.151			
76	951.8	4.58	-0.172	948.4	4.58	-0.171				1011.8	4.63	0.115	1009.8	4.62	0.1147			
78	958.3	4.57	0.114	955.0	4.56	0.094				1021.0	4.63	-0.054	1018.5	4.63	-0.053			
80	965.0	4.58	0.041	961.4	4.57	0.037				1032.4	4.65	0.073	1029.3	4.64	0.0757			
82	972.2	4.59	0.001	967.9	4.59	0.001				1041.5	4.65	0.001	1037.8	4.65	0.0017			
84	973.6	4.60	0.005	969.4	4.60	0.014				1044.5	4.66	0.027	1040.9	4.67	0.0427			
86	975.5	4.62	0.118	971.3	4.61	0.109				1048.6	4.69	0.130	1044.9	4.69	0.1317			

tain value of  $\beta_2$ . The  $\beta_2$  for the ground state is not same for all isotopes of  $Zr$  (see Table. I). For example, the ground state solutions for  $^{82}\text{Zr}$ ,  $^{90}\text{Zr}$ ,  $^{110,120}\text{Zr}$  and  $^{120}\text{Zr}$  are  $\sim -0.2, 0.0, 0.4$  and  $0.0$ , respectively. One can find similar nature for both the force parameter, hence one can conclude that the ground state properties of these nuclei are quite independent of the force parameters used.

## B. Nuclear Binding energy and quadrupole deformation

The calculations mainly explain the nuclear structure as well as the sub-structure properties, based on the basic ingredients such as binding energy ( $E_B$ ), quadrupole moment  $Q_{20}$ , nucleonic density distribution  $\rho(r_\perp, z) = \rho_p(r_\perp, z) +$

$\rho_n(r_\perp, z)$ , and  $rms$  nuclear radii etc. Nevertheless, the present study demonstrates the applicability of RMF on the nuclear structure study for transition nuclei near neutron drip-line. The obtained results for binding energy  $BE$ , quadrupole deformation parameter  $\beta_2$  and the charge radius  $r_{ch}$  for NL3 and NL3\* force parameter for the isotopic chain of  $Zr$ ,  $Mo$ ,  $Ru$  and  $Pd$  are listed in Table-I along with the experimental data [54]. We notice on the binding energy and the  $rms$   $r_{ch}$  for all nuclei over the isotopic chain from RMF agree well with the experimental values. Quantitatively, the mean deviation of  $BE$  and  $r_{ch}$  between the calculated result and the available experimental data over the isotopic chain are  $\sim 0.01$  and  $0.004$ , respectively. Further, the quadrupole deformation parameter  $\beta_2$ , for both ground ( $g.s.$ ) and selective excited states ( $e.s.$ ) are also given in Table I. In some of the earlier RMF and

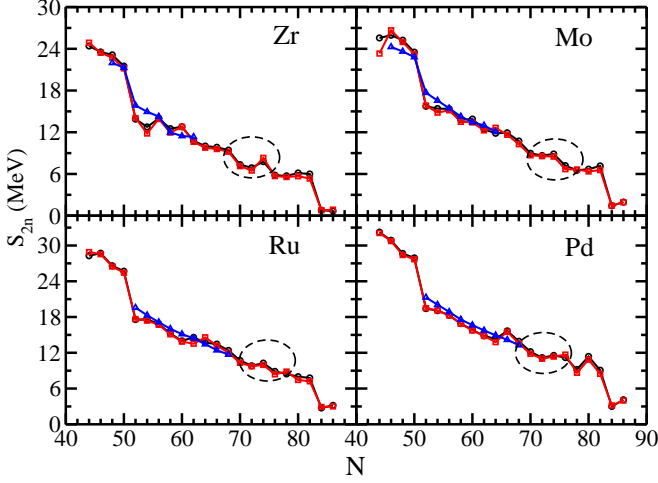


FIG. 2: (Color online) The two neutron separation energy as a function of neutron number from RMF theory with  $NL3$  and  $NL3^*$  force parameter for  $^{82-126}\text{Zr}$ ,  $^{84-128}\text{Mo}$ ,  $^{86-130}\text{Ru}$  and  $^{88-132}\text{Pd}$  nuclei are compared with the experimental data [54].

Skyrme Hartree-Fock (SHF) calculations, it was shown that the quadrupole moment obtained from these theories reproduce the experimental data pretty well [30, 32, 33, 46, 48, 55–57]. From the table, one can find that the shape of few nuclei are not consistent with the experimental observed shape. In this context, we have also estimated the first excited state solution for these nuclei correspond to the experimental deformations (see Table-I). A careful inspection to these solutions shows that the small difference in the binding energy is an indication of shape coexistence. In other words, the two solutions in these nuclei are almost degenerate and might have large shape fluctuations. For example, in  $^{82}\text{Zr}$  the two solutions for  $\beta_2 = -0.197$  and  $\beta_2 = 0.25$  are completely degenerate with binding energies of 691.3 and 691.0 MeV, respectively. Hence, the ground state can be changed to the excited state and vice versa by a small change in the input, like the pairing strength, etc., in the calculations. Similar behavior are also observed for few other nucleus are listed in Table- I. Such phenomenon is known to exist in many other regions [58, 59] of the nuclear chart.

### C. Two neutron separation energy $S_{2n}(Z, N)$

Two neutron separation energy  $S_{2n}(Z, N)$ , can be estimated from the ground state nuclear binding energies of  $BE(Z, N)$ ,  $BE(Z, N-2)$  and the neutron mass  $m_n$  with the relation:

$$S_{2n}(Z, N) = -BE(Z, N) + BE(Z, N-2) + 2m_n, \quad (5)$$

The  $BE$  of the  $^AX_Z$  and  $^{A-2}X_Z$  are calculated from RMF for  $NL3$  and  $NL3^*$  force parameters. It is essential to have very precise mass measurements to predict the correct estimation of the nucleon separation energy  $S_{2n}$ . The calculated  $S_{2n}$  energy from RMF as a function of neutron number for  $Zr$ ,  $Mo$ ,  $Ru$  and  $Pd$  isotopes are compared with latest experimental

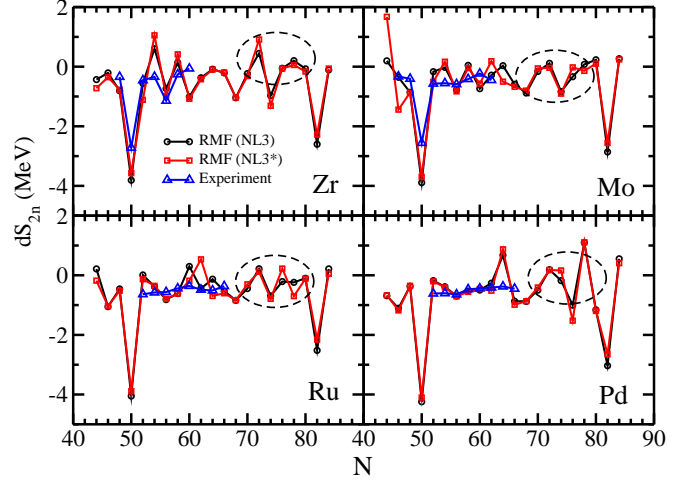


FIG. 3: (Color online) The differential variation of the two neutron separation energy  $dS_{2n}$  as a function of neutron number from RMF theory with  $NL3$  and  $NL3^*$  force parameter for  $^{82-126}\text{Zr}$ ,  $^{84-128}\text{Mo}$ ,  $^{86-130}\text{Ru}$  and  $^{88-132}\text{Pd}$  nuclei are compared with the experimental data [54].

data [54], shown in the Fig. 2. From the figure it is clear that in an isotopic chain, the  $S_{2n}$  energy shows the well-known regularities for a given atomic number i.e. the  $S_{2n}$  decreases smoothly as the number of neutron increases in an isotopic chain. A sharp discontinuities (in other word kinks) appears at neutron magic numbers at  $N = 50$  and  $82$ . In energy terminology, one can write, the energy necessary to remove two neutrons from a nucleus  $(Z, N_{magic}+2)$  is much smaller than that to remove *two* neutrons from the nucleus  $(Z, N_{magic})$ , which breaks the regular trend.

### D. Differential variation of two neutron separation energy

The differential variation of the two neutron separation energy ( $S_{2n}$ ) with respect to neutron number ( $N$ ) i.e.  $dS_{2n}(N, Z)$  is defined as

$$dS_{2n}(Z, N) = \frac{S_{2n}(Z, N+2) - S_{2n}(Z, N)}{2}, \quad (6)$$

The  $dS_{2n}(N, Z)$  is one of the key quantity to explore the rate of change of separation energy with respect to the neutron number in an isotopic chain. Here, we are calculated the  $dS_{2n}(N, Z)$  for  $NL3$  &  $NL3^*$  force parameter. Further, we have also estimated the  $dS_{2n}(N, Z)$  energy from the experimental  $S_{2n}$  energy. In Fig. 3, we are compared the experimental values with our calculation for  $Zr$ ,  $Mo$ ,  $Ru$  and  $Pd$  isotopes. In general, the large sharp deep fall in the  $dS_{2n}$  over an isotopic chain shows the signature of neutron shell closure. In other word, this deviation in the general trend may disclose some additional nuclear structure features. From the figure, we observed the same characteristics for all  $Z=38-46$ .

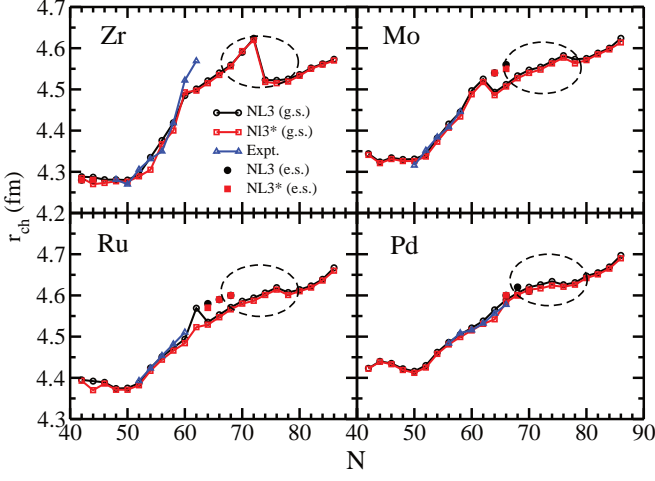


FIG. 4: (Color online) The root-mean-square charge distribution  $r_{ch}$  of  $^{82-126}\text{Zr}$ ,  $^{84-128}\text{Mo}$ ,  $^{86-130}\text{Ru}$  and  $^{88-132}\text{Pd}$  nuclei from RMF theory with  $NL3$  and  $NL3^*$  force parameter are compared with the experimental data [61].

### E. The root-mean-square charge distributions

The root mean square (*rms*) matter radius from relativistic mean field theory can be expressed as:

$$\langle r_m^2 \rangle = \frac{1}{A} \int \rho(r_{\perp}, z) r^2 d\tau, \quad (7)$$

where  $A$  is the mass number and  $\rho(r_{\perp}, z)$  is the axially deformed density. The *rms* charge radius can be calculated from the *rms* proton radius  $\langle r_p^2 \rangle$  with simple algebraic relation,

$$\langle r_{ch}^2 \rangle = \langle r_p^2 \rangle + 0.64. \quad (8)$$

From the theoretical point of view, the *macroscopic-microscopic* models [60] and *microscopic* mean-field formulations using effective interactions are most sophisticated approaches to determine the *rms* charge radius in comparison with experimental data [61]. In this present work, we have shown the variations or fluctuations of the charge radii on the top of a fairly smooth average behavior in an isotopic chain. The results from RMF approaches for  $NL3$  and  $NL3^*$  parameters along with the available experimental datas are shown in Fig. 4. From the figure it is clear that the obtained radii from RMF for  $^{82-126}\text{Zr}$ ,  $^{84-128}\text{Mo}$ ,  $^{86-130}\text{Ru}$  and  $^{88-132}\text{Pd}$  follows closely the experimental data [61]. For most of the nuclei, the experimental values are unavailable, the RMF prediction are made for the charge radius of such a nucleus that awaits experimental confirmation. The circle, square and triangle symbols indicate the ground state states data for  $NL3$ ,  $NL3^*$  and experiment. Further, the solid circle and solid square symbols indicate the shapes corresponds to the first intrinsic excited states obtained from  $NL3$  and  $NL3^*$  force, respectively. From the figure, one can observe the smooth behavior for lighter isotopes, then there is a small fall in the charge radii for Zr, Mo, and Pd at about  $N=62, 64, 72$  and

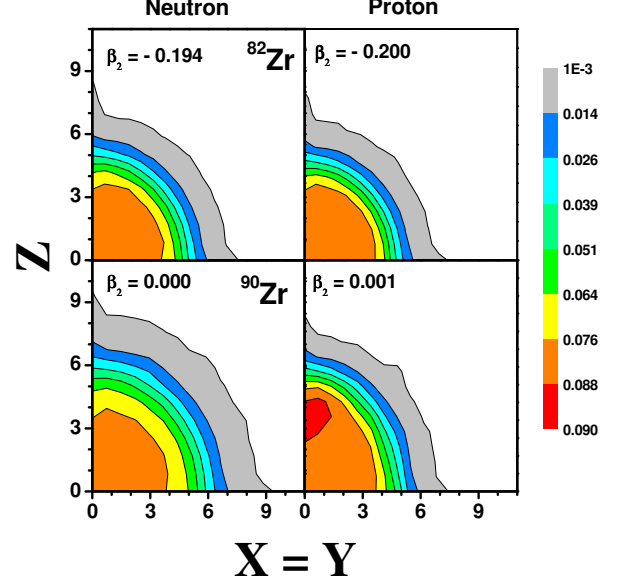


FIG. 5: (Color online) The potential energy surface of  $^{112}\text{Ba}$  as a function of quadrupole deformation parameter  $\beta_2$  for both constant gap  $\Delta_{n,p}$  and constant strength  $G$ , approximation of BCS theory in axially deformed RMF calculations using  $NL3$  parameter set.

74. These fall corresponds to the transition from the prolate to the oblate and vice versa. But the magnitude for both the states are different, i.e., the oblate deformation is at  $\beta_2 \sim -0.2$  while the prolate one appears with  $\beta_2 \sim 0.4$ . In case of  $Pb$  isotope, the change is the radii only at one place i.e. at  $N=74$ . Further, one can notice that the tiny change in the calculation can lead to the first intrinsic excited state as ground state (see Fig. 1). In other word, we can practically degenerate the ground state binding energy for the deformation corresponding to the first intrinsic excited state. Thus, the inconsistency in the  $r_c^2$  could be explain in terms of configuration mixing i.e the actual ground state is not only the spherical configuration but also from the neighbor deformed intrinsic excited states.

### F. The contour plot of the axially deformed density distributions

In the above figures and tables, we have shown the results for few structural observables such as binding energy, quadrupole deformation, rms radius, separation energy and differential separation energy in comparison with the experimental data [54, 61]. Based on the experimental data, we have focused on the ground of  $^{82-126}\text{Zr}$ ,  $^{84-128}\text{Mo}$ ,  $^{86-130}\text{Ru}$  and  $^{88-132}\text{Pd}$  nuclei along with few selective excited states. Overall, we found some significant signature of shell closure at  $N = 50$  and  $82$  in the isotopic chains. Further, the abnormal variation of  $S_{2n}$  and  $dS_{2n}$  near  $N \sim 64$  and  $74$  in Zr,

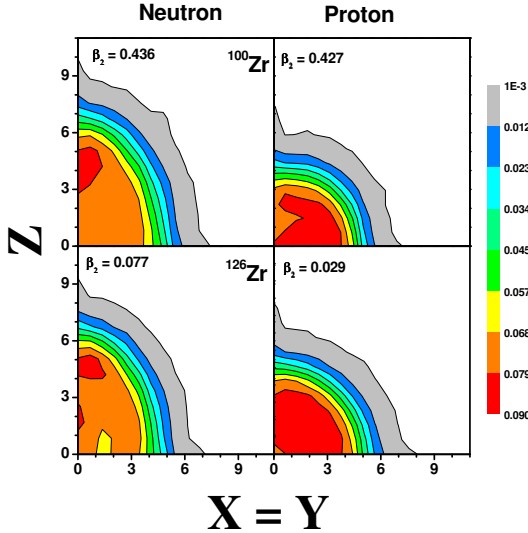


FIG. 6: (Color online) The potential energy surface of  $^{112}\text{Ba}$  as a function of quadrupole deformation parameter  $\beta_2$  for both constant gap  $\Delta_{n,p}$  and constant strength  $G$ , approximation of BCS theory in axially deformed RMF calculations using NL3 parameter set.

*Mo* and *Ru* isotopes suggests a shape co-existence. A more careful inspection shows that the tendency of abnormality in the  $S_{2n}$  and  $dS_{2n}$  are decreased in the isotonic chain. In other word, we get a smoother behavior in neutron separation energy for *Pd* nuclei in comparison to *Zr* isotopes. The divergence can be cut down by taking the dynamical correlations beyond mean field [62–64].

To get a complete picture into the reason behind such discrepancy over the isotopic chain, we have shown the contour plot of axially deformed density of proton and neutron of these nuclei. In FIG. 4, we have displayed the distribution of *Zr* isotopes for  $N=42, 50, 60$  and  $82$  as representative cases. All the isotopes of *Mo*, *Ru* and *Pd* also showing similar behavior as *Zr* as shown in FIG. 4. From the figure, one can clear identify the spherical, oblate, prolate shapes corresponding to their  $\beta_2$  values as the local minima in the PECs. Similar calculations can also be found in Ref. [65, 66]. In these figures we can

see that the transition from oblate to prolate at  $N=42$ , then change to the spherical structure at  $N=50$  and further changing the deformations to prolate one. Even the proton number is fixed in the isotopic chain, still we found a little change in the density distribution due to the influence of excess neutron number. Following the color code, the red and light grey color corresponding to the high density ( $\sim 0.09 \text{ fm}^{-3}$ ) and low density ( $\sim 0.001 \text{ fm}^{-3}$ ), respectively. More inspection on the figures shows that the central density of the proton increases as compared to the neutron with respect to the neutron number. In this region, few isotopes of *Mo* (for  $^{116-118}\text{Mo}$ ) are triaxial shape in their ground state, which is very close to the axial solutions [66]. In other word, the location of minima for triaxial solution for these isotopes of *Mo* are almost same as the minima appear for axial prolate axial solution. Hence, we have used the simple axial deformed calculation, which is good enough for the a qualitative descriptions of structural observables in this mass region.

#### IV. SUMMARY AND CONCLUSIONS

We have used self-consistent relativistic mean field theory with most popular *NL3* and recent *NL3\** force parameters to study the structural evolution in transition nuclei. The conjecture has been made from the neutron separation energies, differential variation of separation energy and the root-mean-square charge radii of these nuclei. In this present calculations we have shown that *Zr*, *Mo* and *Sr* isotopes undergo a transition from oblate to prolate shapes at  $N \sim 64$  and  $74$ . But, in case of *Pd* follows a smooth pattern through out the isotopic chain. We have also shown the dependence of nuclear charge radii on deformation also play an crucial role on their structural transition. Further, we have also observed a large shell gap at  $N = 82$ , almost same in magnitude at  $N=50$  for these considered nuclei, which is a well-known feature for mean-field calculation. We have also demonstrated the efficiency of RMF theory calculations to reproduce those features and therefore to make predictions in unexplored regions.

#### Acknowledgments

The author thanks to Shan-Gui Zhou, Cheng-Jun Xia, Jie Zhao, Bing Wang and Zhen-Hua Zhang for various discussion and also for careful reading of the manuscript.

- [1] M. Pfützner, M. Karny, L. Grigorenko, and K. Riisager, Rev. Mod. Phys. **84**, 567 (2012).
- [2] B. Blank and M. Borge, Prog. Part. Nucl. Phys. **60**, 403 (2008).
- [3] E. Olsen, M. Pfützner, N. Birge, M. Brown, W. Nazarewicz and A. Perhac, Phys. Rev. Lett. **110**, 222501 (2013).
- [4] H. J. Rose and G. A. Jones, Nature **307**, 245 (1984).
- [5] Raj K. Gupta and W. Greiner, Int. J. Mod.Phys. **3**, 335 (1994).

- [6] B. B. Singh, M. Bhuyan, S. K. Patra and Raj K. Gupta, J. Phys. G:Nucl. Part. Phys **39**, 025101 (2012).
- [7] L. P. Gaffney *et al.* Nature **497**, 199 (2013).
- [8] C. J. (Kim) Lister and Jonathan Butterworth, Nature **497**, 190 (2013).
- [9] C. Thibault *et al.*, Phys. Rev. C **12**, 644 (1975).
- [10] O. B. Tarasov *et al.*, Phys. Rev. Lett. **102** 142501 (2009).



- [11] T. Ohnishi *et al.*, J. Phys. Soc. Jpn. **77**, 083201 (2008).
- [12] T. Ohnishi *et al.*, J. Phys. Soc. Jpn. **79**, 073201 (2010).
- [13] H. Watanabe *et al.*, Phys. Rev. Lett. **111**, 152501 (2013).
- [14] J. Meng and P. Ring, Phys. Rev. Lett. **80**, 460 (1998).
- [15] H. Iwasaki *et al.*, Phys. Lett. B **481**, 7 (2000).
- [16] T. Motobayashi *et al.*, Phys. Lett. B **346**, 9 (1995).
- [17] B. Bastin *et al.*, Phys. Rev. Lett. **99**, 022503 (2007).
- [18] M. G. Mayer, Phys. Rev. **75**, 1969 (1949).
- [19] J. Blons, Nucl. Phys. A **502**, 121 (1989).
- [20] T. Sumikama, K. Yoshinaga, H. Watanabe, S. Nishimura, Y. Miyashita, K. Yamaguchi, K. Sugimoto, J. Chiba, Z. Li, H. Baba *et al.*, Phys. Rev. Lett. **106**, 202501 (2011).
- [21] K.-L. Kratz, B. Pfeiffer, O. Arndt, S. Hennrich, and A. Wöhr (t ISOLDE/IS333 Collaboration and IS393 Collaboration), Eur. Phys. J. A **25**, 633 (2005).
- [22] S. Nishimura, Prog. Theor. Exp. Phys. **2012**, 03C006 (2012).
- [23] X. L. Tu *et al.*, Phys. Rev. Lett. **106**, 112501 (2011).
- [24] Y. H. Zhang *et al.*, Phys. Rev. Lett. **109**, 102501 (2012).
- [25] W. D. Myers, Nucl. Phys. A **145**, 387 (1970).
- [26] W. D. Myers, K. H. Schmidt, Nucl. Phys. A **410**, 61 (1983).
- [27] I. Tanihata, H. Hamagaki, O. Hashimoto, Y. Shida, N. Yoshikawa, K. Sugimoto, O. Yamakawa, K. Tobayashi, N. Takahashi, Phys. Rev. Lett. **55**, 2676 (1985).
- [28] M. Lassaut and R.J. Lombard, Z. Phys. A **341**, 125 (1992).
- [29] W. Pannert, P. Ring, and J. Boguta, Phys. Rev. Lett., **59**, 2420, (1986).
- [30] B. D. Serot and J. D. Walecka, Adv. Nucl. Phys. **16**, 1 (1986).
- [31] J. Boguta and A. R. Bodmer, Nucl. Phys. A **292**, 413 (1977).
- [32] S. K. Patra, M. Bhuyan, M. S. Mehta and Raj K. Gupta, Phys. Rev. C **80**, 034312 (2009).
- [33] M. Bhuyan, S. K. Patra, and Raj K. Gupta, Phys. Rev. C **84**, 014317 (2011).
- [34] P. G. Reinhard, Rep. Prog. Phys. **52**, 439 (1989).
- [35] P. Ring, Prog. Part. Nucl. Phys. **37**, 193 (1996).
- [36] D. Vretenar, A. V. Afanasjev, G. A. Lalazissis, and P. Ring, Phys. Rep. **409**, 101 (2005).
- [37] J. Meng, H. Toki, S. G. Zhou, S. Q. Zhang, W. H. Long, and L. S. Geng, Prog. Part. Nucl. Phys. **57**, 470 (2006).
- [38] N. Paar, D. Vretenar, and G. Colo, Rep. Prog. Phys. **70**, 691 (2007).
- [39] T. Niksić, D. Vretenar, and P. Ring, Prog. Part. Nucl. Phys. **66**, 519 (2011).
- [40] C. J. Horowitz and B. D. Serot, Nucl. Phys. A **368**, 503 (1981).
- [41] J. Boguta, Nucl. Phys. A **372**, 386 (1981).
- [42] C. E. Price, G. E. Walker, Phys. Rev. C **36**, 354 (1987).
- [43] J. Fink, V. Blum, P.-G. Reinhard, J. A. Maruhn, W. Greiner, Phys. Lett. B **218**, 277 (1989).
- [44] D. G. Madland and J. R. Nix, Nucl. Phys. A **476**, 1 (1981).
- [45] P. Möller and J.R. Nix, At. Data and Nucl. Data Tables **39**, 213 (1988).
- [46] G. A. Lalazissis, J. König, and P. Ring, Phys. Rev. C **55**, 540 (1997).
- [47] G. A. Lalazissis, S. Karatzikos, R. Fossion, D. Pena Arteaga, A. V. Afanasjev, P. Ring, Phys. Lett. B **671**, 36 (2009).
- [48] Y. K. Gambhir, P. Ring, and A. Thimet, Ann. Phys. (N.Y.) **198**, 132 (1990).
- [49] N. Dubray, H. Goutte and J. -P. Delaroche, Phys. Rev. C **77**, 014310 (2008).
- [50] J. Fink, V. Blum, P. -G. Reinhard, J. A. Maruhn, and W. Greiner, Phys. Lett. B **218**, 277 (1989).
- [51] D. Hirata, H. Toki, I. Tanihata, and P. Ring, Phys. Lett. B **314**, 168 (1993).
- [52] B. N. Lu, J. Zhao, E. G. Zhao, S. G. Zhou, Phys. Rev. C **89**, 014323 (2014).
- [53] S. Karatzikos, A. V. Afanasjev, G. A. Lalazissis, P. Ring, Phys. Lett. B **689**, 72 (2010).
- [54] M. Wang, G. Audi, A. H. Wapstra, F. G. Kondev, M. McCormick, X. Xu and B. Pfeiffer, Chen. Phys. C **36**, 1603 (2012).
- [55] B. A. Brown, Phys. Rev. C **58**, 220 (1998).
- [56] S. K. Patra, C. -L. Wu, C. R. Prahara, and R. K. Gupta, Nucl. Phys. A **651**, 117 (1999).
- [57] P. Arumugam, B. K. Sharma, S. K. Patra, and R. K. Gupta, Phys. Rev. C **71**, 064308 (2005).
- [58] S. Yoshida, S. K. Patra, N. Takigawa, and C. R. Prahara, Phys. Rev. C **50**, 1398 (1994).
- [59] S. K. Patra, S. Yoshida, N. Takigawa, and C. R. Prahara, *ibid.* **50**, 1924 (1994).
- [60] J. S. Wang, W. Q. Shena, Z. Y. Zhua, J. Feng, Z. Y. Guob, W. L. Zhan, G. Q.Xiao, X. Z. Cai, D. Q. Fang, H. Y. Zhang, Y. G. Ma, Nucl. Phys. A **691**, 618 (2001).
- [61] I. Angeli, K.P. Marinova, Atomic Data and Nucl. Data Tables **99**, 69 (2013).
- [62] M. Bender, G. F. Bertsch, P. -H. Heenen, Phys. Rev. C **73**, 034322 (2006).
- [63] M. Bender, G. F. Bertsch, P. -H. Heenen, Phys. Rev. C **78**, 054312 (2008).
- [64] J. -P. Delaroche *et al.*, Phys. Rev. C **81**, 014303 (2010).
- [65] E. Bauge *et al.*, Euro. Phys. J. A **48**, 113 (2012); [www-phynu.cea.fr](http://www-phynu.cea.fr).
- [66] R. Rodriguez-Guzmn, P. Sarriguren, L.M. Robledob, and S. Perez-Martin, Phys. Lett. B **691**, 202 (2010).